Insight into the Bind−Lock Mechanism of the Yeast Mitochondrial ATP Synthase Inhibitory Peptide

Vincent Corvest, Claude Sigalat, and Francis Haraux*

Institut de Biologie et de Technologie de Saclay and CNRS-URA 2096, CEA Saclay, F 91191 Gif-sur-Yvette, France

Received March 15, 2007; Revised Manuscript Received May 24, 2007

ABSTRACT: The mechanism of yeast mitochondrial F_1-ATPase inhibition by its regulatory peptide IF1 was investigated with the noncatalytic sites frozen by pyrophosphate pretreatment that mimics filling by ATP. This allowed for confirmation of the mismatch between catalytic site occupancy and IF1 binding rate without the kinetic restriction due to slow ATP binding to the noncatalytic sites. These data strengthen the previously proposed two-step mechanism, where IF1 loose binding is determined by the catalytic state and IF1 locking is turnover-dependent and competes with IF1 release (Corvest, V., Sigalat, C., Venard, R., Falson, P., Mueller, D. M., and Haraux, F. (2005) *J. Biol. Chem*. *280*, 9927−9936). They also demonstrate that noncatalytic sites, which slightly modulate IF1 access to the enzyme, play a minor role in its binding. It is also shown that loose binding of IF1 to MgADP-loaded F_1-ATPase is very slow and that IF1 binding to ATP-hydrolyzing F_1-ATPase decreases nucleotide binding severely in the micromolar range and moderately in the submillimolar range. Taken together, these observations suggest an outline of the total inhibition process. During the first catalytic cycle, IF1 loosely binds to a catalytic site with newly bound ATP and is locked when ATP is hydrolyzed at a second site. During the second cycle, blocking of ATP hydrolysis by IF1 inhibits ATP from becoming entrapped on the third site and, at high ATP concentrations, also inhibits ADP release from the second site. This model also provides a clue for understanding why IF1 does not bind ATP synthase during ATP synthesis.

ATP synthases (also called F_0F_1-ATPases[1]) are enzymatic complexes anchored to bacterial cytoplasmic membranes, mitochondrial inner membranes, and chloroplast thylakoid membranes (*1*). They have also been found associated to plasma membranes of endothelial cells (*2*). These enzymes couple the condensation of ADP and inorganic phosphate into ATP to the dissipation of the protonmotive force (pmf) generated by redox processes (*3*−*4*). ATP synthases, composed of an extrinsic F_1 domain ($\alpha_3\beta_3\gamma\delta\epsilon$) and of a membranous F_0 domain connected by a central axis and a peripheral stalk (*5*−*7*), are rotary molecular motors (*8*−*9*). The pmf drives the rotation of a membranous oligomer of c subunits. This turbine transmits its movements to the central axis ($\gamma\delta\epsilon$ in mitochondria) that penetrates the catalytic domain. Rotation of this asymmetrical axis sequentially distorts the three catalytic sites located at three interfaces of the $\alpha_3\beta_3$ heterohexamer, driving ATP synthesis (*1*). The $\alpha_3\beta_3$ hexamer also contains three noncatalytic nucleotide binding sites (*10*), the role of which is controversial (*11*−*16*). Rotation of the central axis has been directly observed in a number of single molecule experiments (*9*, *17*−*18*), and the relationship between angular motion and the main catalytic steps has been established (*17*−*18*).

Mitochondrial ATP synthase is regulated by an inhibitory peptide called IF1, discovered in animal mitochondria (*19*) and later found in yeast (*20*) and plants (*21*). IF1 is a soluble peptide, 84 residues-long in bovine and 63 residues-long in yeast. Its structure is essentially α-helical (*22*). When the pmf collapses, which happens during anoxia or particular events making the inner mitochondrial membrane permeable to H^+ ions, IF1 binds the catalytic sector of ATP synthase and inhibits ATP hydrolysis (reviewed in ref *23*). When the pmf is applied again, IF1 is released (*23*−*31*), possibly after passing through an intermediate, non-inhibitory position (*32*−*34*). IF1 binds the solubilized catalytic sector (MF_1) as well as the membrane-bound enzyme. IF1 and MF_1 have been crystallized together, and the inhibitory peptide was found associated by its N-terminal part to one of the three catalytic α/β interfaces (*35*). This interface was expected to contain ADP according to previous structures (*5*, *36*) but actually contained ATP or perhaps its analogue AMP-PNP. This structure is thought to be that of the dead-end, inhibited complex.

IF1 binding is a dynamic process that requires MgATP and exclusively occurs during catalytic turnover (*30*, *37*). To understand the mechanism of inhibition, it is therefore necessary to know if different steps separate IF1 binding and the formation of the dead-end complex. This is also a prerequisite for understanding the reverse process, that is the pmf-induced release of IF1. The first approach consists in studying, at variable ATP concentrations, the relationship

* To whom correspondence should be addressed. Tel: 33 1 69 08 98 91. Fax: 33 1 69 08 87 17. E-mail: francis.haraux@cea.fr.

[1] Abbreviations: F_0F_1, ATP synthase complex (EC 3.6.3.14); F_0, membranous sector of ATP synthase; F_1, catalytic sector of ATP synthase; IF1, endogenous inhibitory peptide of ATP synthase; pmf, protonmotive force; AMP-PNP, adenylyl-imidodiphosphate; EDTA, ethylenediaminetetraacetic acid; LDH, lactate dehydrogenase; MES, 2-(*N*-morpholino)ethane sulfonic acid; Ni-NTA, nickel-nitrilotriacetic acid; Pi, inorganic phosphate; PK, pyruvate kinase; PP_i, inorganic pyrophosphate; Tris, tris (hydroxymethyl) aminomethane.

10.1021/bi700522v CCC: $37.00
Published on Web 06/27/2007

between the catalytic site occupancy and the rate of IF1 binding, the latter being an indication of the accessibility of the binding site. A complex relationship was found between ATP concentration and the rate of IF1 binding to isolated bovine F_1-ATPase (*38*). We found the same relationship with yeast F_1-ATPase, and we probed in parallel the nucleotide occupancy of catalytic sites by fluorescence quenching of a tryptophan, which was engineered in the catalytic site (βY345W) (*39*). By the combination of fluorescence and kinetic data, we estimated that the variation of the rate of IF1 binding did not follow the filling of catalytic sites, which means that the accessibility of the IF1 binding site is not strictly controlled by the catalytic state of the enzyme. To explain this result, we proposed a two-step bind−lock mechanism, in which loose binding of IF1 is controlled by the catalytic state of F_1-ATPase, and locking of IF1 is turnover-dependent. However, the nucleotide occupancy of the noncatalytic sites, which also varies with ATP concentration, was not controlled in these experiments, and we do not know whether the conformation of noncatalytic sites may affect IF1 binding. Moreover, when the noncatalytic sites are not initially filled with ATP, a lag phase of several minutes precedes the steady-state regime of ATP hydrolysis, except for MgATP concentrations below 5−10 μM and above 0.5−1 mM (*39*). Because the fluorescence measurement of nucleotide occupancy should be done a few seconds after MgATP addition in order to avoid substrate exhaustion, we could do it only at two MgATP concentrations (1 μM and 1 mM), and estimates of nucleotide occupancy at other concentrations were indirect. The present work overcame the possible influence of noncatalytic sites on IF1 binding. Using pyrophosphate pretreatment, we froze the noncatalytic sites of yeast F_1-ATPase in a state that mimics their filling with ATP (*13*, *40*). We then obtained constant ATP hydrolysis immediately after substrate addition, which allowed us to correlate the quenching of βW345 fluorescence, ATPase activity, and the IF1 binding rate for MgATP concentrations ranging from 30 nM to 5 mM. With the noncatalytic sites so frozen, we still observed that the rate of IF1 binding was not determined by nucleotide occupancy of the catalytic sites, which confirms the hypothesis of a two-step mechanism. The pyrophosphate pretreatment increased the rate of IF1 binding a little, indicating that noncatalytic sites have a measurable but limited influence on the accessibility of the IF1 binding site. We also obtained experimental evidence that IF1 probably does not significantly bind to a catalytic site containing ADP, showing that bound IF1 decreases the catalytic site occupancy, and therefore could propose a model where the role of the different catalytic intermediates and steps in IF1 binding and locking is explicit.

MATERIALS AND METHODS

Molecular Biology. DNA manipulations were carried out following published procedures (*41*). The gene encoding the β-subunit (*ATP2*) was amplified by polymerase chain reaction (PCR) from plasmid pRS344SB (*42*) kindly provided by Dr. David M. Mueller (Chicago, IL). The PCR fragment was ligated into plasmid pRS313 forming pRS313/atp2-Y345W. Codons encoding the His_{10}-tag were inserted between the sequence of the leader peptide and the sequence of the mature β-subunit by directed mutagenesis. pRS313/atp2-Y345W and primers containing 10 histidine codons (CAC $(CAT)_4$CAC $(CAT)_4$) were used with QuikChange Site-Directed Mutagenesis Kit from Stratagene (La Jolla, CA) to obtain pRS313/atp2-H_{10}-Y345W. Restriction and DNA modification enzymes were purchased from New England Biolabs (Frankfurt, Germany). DNA was prepared and purified using kits obtained from Qiagen (Qiagen GmbH, Hilden, Germany). Plasmids were amplified in *E. coli* DH5αMCR after transformation by electroporation using a Biorad (Hercules, CA) Gene Pulser electroporator with the method recommended by the manufacturer.

Yeast Strains and Growth Conditions. Saccharomyces cerevisiae cells (Euroscarf BY4741-Δ*atp2 MAT a*, *his3Δ1*, *leu2Δ0*, *met15Δ0*, *ura3Δ0*, and *atp2::kanMX4*) were transformed with the plasmid pRS313/atp2-H_{10}-Y345W as described (*43*). Transformed cells were selected on a strictly respiratory medium containing 1% yeast extract, 0.1% KH_2PO_4, 0.12% $SO_4(NH_4)_2$, and 2% lactate at pH 5.5 (28 °C). Transformed cells and WT cells (Euroscarf BY4741 *MAT a*, *his3Δ1*, *leu2Δ0*, *met15Δ0*, and *ura3Δ0*) were grown at 28 °C in a large volume of strictly respiratory medium. Yeast extract was from Difco (Detroit, MI), and others chemicals were from Sigma Chemical Co. (St. Louis, MO).

Purification of Nucleotide-Depleted His_{10}-Tagged F_1-ATPase. Yeast mitochondrial F_1-ATPase (MF_1) was purified using a prior method (*39*, *44*) with the following modifications. After chloroform extraction and precipitation with 70% saturated $SO_4(NH_4)_2$, the pellet was dissolved in 2 mL of binding buffer (BB) (10 mM imidazole, 0.3 mM NaCl, and 50 mM Na_2HPO_4 at pH 8). The sample was incubated, under gentle stirring, with 3 mL of Ni-NTA resin (Qiagen GmbH, Hilden, Germany) prepared in BB. The resin was poured into a 0.9 cm diameter column, and the column was washed sequentially with 5 and 2 volumes of the BB containing imidazole at 10 and 20 mM, respectively. MF_1 was eluted by gravity with 2 volumes of BB containing 250 mM imidazole. The fractions containing MF_1 were pooled and dialyzed at room temperature for 2 h against a buffer containing 30 mM Tris-SO_4 and 1 mM EDTA at pH 7.5 (TE). The sample was precipitated with 70% saturated $SO_4(NH_4)_2$, centrifuged, and dissolved in a minimal volume of TE containing 70% saturated $SO_4(NH_4)_2$. The nucleotide (ATP and ADP) content of the enzyme was estimated, after denaturation, to less than 0.01 mol/mol using a luciferase assay (*45*), where ADP was converted into ATP with phosphoenolpyruvate and pyruvate kinase. The rate of ATP hydrolysis was measured at pH 6.5 and 25 °C in the presence of 1 mM MgATP. The turnover number for ATP hydrolysis was 400 s^{-1} for the wild type F_1-ATPase and 280 s^{-1} for βY345W F_1-ATPase, on the basis of a molecular mass of 372 kDa.

Pretreatment with Pyrophosphate. MF_1 (1−5 μM) was incubated at room temperature in a buffer containing 20 mM Tris (HCl) (pH 7.5), 30% glycerol, 2 mM K-pyrophosphate, and 2.5 mM $MgCl_2$. The effect of pyrophosphate, checked by the absence of lag in the kinetics of ATP hydrolysis, was complete after 15 min and stable for at least 7−8 h.

Overexpression and Purification of IF1. Because of the presence of the N-terminal enterokinase cleavage site, the first three amino acids of the recombinant enzyme were Ala-Met-Ala, as compared to the natural IF1, which starts with Ser (*39*). In addition, Phe27 and Phe28 were replaced by Trp to facilitate the detection of the protein during elution.

These mutations did not alter the inhibitory properties of the peptide. This overexpressed peptide was used for kinetic experiments.

Stock solutions of concentrated IF1 contained 0.01% Tween-20 to prevent adsorption of the protein on plasticware. After dilution in the spectrophotometric cuvette, Tween-20 alone had no effect on F_1-ATPase activity.

Protein Titration. Protein concentration was determined using a micro-BCA titration kit (Pierce Chemical Co., Rockford, IL).

Fluorescence Measurement and Analysis. Fluorescence measurements (excitation, 295 nm; emission, 350 nm; bandwidth, 5 nm) were carried out as previously described (*39*). The cuvette, stirred and thermostatted at 25 °C, was filled with buffer containing 50 mM MES, 20 mM KCl, and 2 mM $MgCl_2$ at pH 6.5. Additions of MF_1 and nucleotides were made as described in the Figure legends at indicated concentrations. Because of ATP consumption, it was crucial to estimate at what time after additions reliable fluorescence measurement could be made. The total procedure of injection resulted in a blind period of 2 s where no reliable measurement could be made, but because of efficient mixing, the final level was reached immediately after this period. This time response was determined from the time-course of fluorescence following a tryptophan injection. To minimize ATP consumption, low concentrations of F_1-ATPase were used (down to 5 nM), and 10 kinetics were averaged to improve the signal-to-noise ratio. Fluorescence during ATP hydrolysis was averaged between $t = 1$ s and $t = 2$ s after MgATP addition, the zero time being the middle of the blind period. Fluorescence values were corrected for the fluorescence of nucleotides, for the dilution effects, and for the inner filter effect of the nucleotides, as in ref *39*. Some measurements were made in the presence of WT IF1, the fluorescence of which was deduced. It was also verified using WT F_1-ATPase that IF1 binding does not affect the fluorescence of F_1-ATPase endogenous tryptophans. Nucleotide binding parameters were calculated by fitting the fluorescence versus nucleotide concentration data to a theoretical curve, using an ordered tri-site model. Contrary to that generally done in the literature, we did not neglect the bound nucleotides in calculations because this approximation is quite inappropriate at low nucleotide concentrations. The concentration [S] of free ligand was therefore given by the equation $[S]^3 + a[S]^2 + b[S] + c$, with $a = 2\,[E_{tot}] + K_{d2} - [S_{tot}]$, $b = K_{d2}\,([E_{tot}] + K_{d1} - [S_{tot}])$, and $c = -K_{d1}K_{d2}\,[S_{tot}]$. The total concentrations of ligand $[S_{tot}]$ and enzyme $[E_{tot}]$ are known, and K_{d1}, K_{d2}, K_{d3} are the three dissociation constants to be determined. By algebraically solving the third degree equation using the classical methods, which gave a single real positive root, [S] was expressed as a function of $[S_{tot}]$, $[E_{tot}]$, K_{d1}, K_{d2}, and K_{d3}. Then, the concentrations of enzymes with one, two, and three bound nucleotides were expressed as a function of $[E_{tot}]$, [S], K_{d1}, K_{d2}, and K_{d3}, and the theoretical fluorescence was expressed as the sum of the concentrations of the different states weighted by their respective fluorescence levels (parameters to be determined). Finally, the root-mean-square deviation between theoretical and experimental fluorescence values was minimized by adjusting the values of the parameters, using the Solver of Microsoft Excel software. It was verified that at high nucleotide concentrations (but not at low concentrations), the model gave values the same as those given by the simpler model that neglects bound nucleotides. Two different cases were considered. In the first case, the contributions of the three catalytic sites to fluorescence quenching were forced to be equal, and in the second case, they were allowed to take distinct values $\Delta F1$, $\Delta F2$, and $\Delta F3$ during the fitting process.

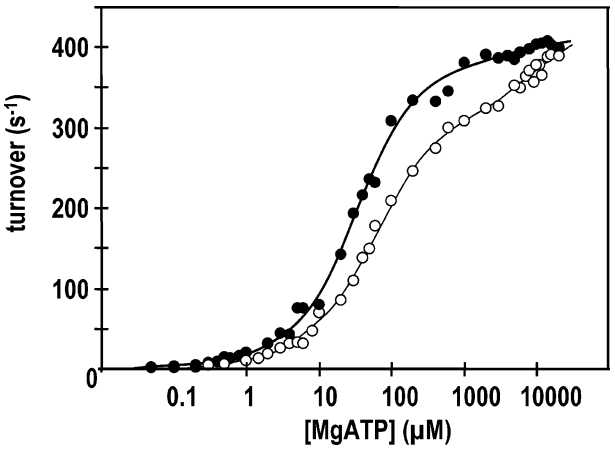

FIGURE 1: Rate of ATP hydrolysis by MF_1-βY345W versus MgATP concentration. Effect of PP_i pretreatment. Conditions are as described under Materials and Methods. (○), control; (●), PP_i pretreated. Enzymes concentrations: 4 nM MF_1-βY345W, 4 U/mL PK, and 10 U/mL LDH at lower MgATP concentrations (submicromolar range), and 2 nM MF_1-βY345W, 20 U/mL PK, and 50 U/mL LDH at higher MgATP concentrations. Each point represents the average of 2−4 measurements made at steady state. Continuous curves were drawn by fitting the data to a model with three distinct classes of catalytic sites, at least one of which is regulatory, with $v = v_1[ES] + v_2[ESS] + v_3[ESSS]$, where v is the catalytic turnover, and ES, ESS, and ESSS are the concentrations of enzymes with 1, 2, and 3 filled catalytic sites. Parameters: $K_1 = 2.9 \pm 2\ \mu M$, $v_1 = 36 \pm 25\ s^{-1}$, $K_2 = 64 \pm 10\ \mu M$, $v_2 = 313 \pm 5\ s^{-1}$, $K_3 = 11.3 \pm 1.8$ mM, and $v_3 = 438 \pm 16\ s^{-1}$ for the control; $K_1 = 0.33 \pm 0.3\ \mu M$, $v_1 = 14 \pm 10\ s^{-1}$, $K_2 = 34 \pm 3\ \mu M$, $v_2 = 383 \pm 9\ s^{-1}$, $K_3 = 10.3 \pm 7.7$ mM, and $v_3 = 417 \pm 23\ s^{-1}$ for the PP_i-pretreated enzyme. See text for details.

ATP Hydrolysis Measurement and Kinetic Analysis. Continuous monitoring of ATP hydrolysis coupled to NADH oxidation was carried out spectrophotometrically as described (*39*). The reaction was observed in a stirred and thermostatted cuvette (25 °C) containing 50 mM MES at pH 6.5, 20 mM KCl, 2 mM $MgCl_2$, 1 mM phosphoenolpyruvate, 20 units/mL pyruvate kinase, 50 units/mL lactate dehydrogenase, and 0.4 mM NADH and MgATP at indicated concentrations. The ATPase reaction was initiated by adding F_1-ATPase at the indicated final concentration (4−10 nM) and monitored by absorbance decrease of NADH at 340 nm. Steady-state ATPase activity varied linearly with MgATP concentrations lower than 1 μM. However, it differed from zero in the absence of added MgATP, the zero value being obtained by extrapolating the data to a slightly negative value of substrate concentration. This is due to contaminating nucleotides contained in the regenerating system (PK/LDH/PEP/NADH), leading to a systematic underestimation of MgATP concentration that was estimated to at most 50 nM in the data in Figures 1 and 2. The consequence on the determination of enzymologic parameters is limited to the low MgATP concentration range and was actually found to be negligible (see Results). After 1−3 min of continuous ATP hydrolysis, IF1 (20 nM) was injected into the cuvette, and ATPase activity decayed. The spectrophotometric recording was

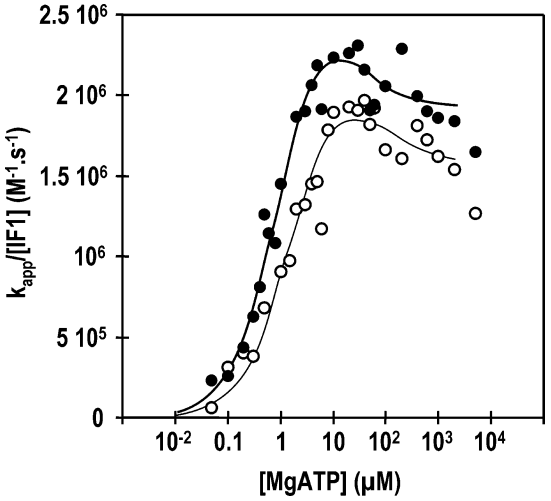

FIGURE 2: IF1 kinetic constant of inhibition vs MgATP concentration. Effect of PP_i pretreatment. Conditions are as described in Figure 1 with 20 nM IF1. (○), control; (●), PP_i pretreated. Each value is the average of 2−4 measurements. Continuous curves are shown with theoretical model with k_{on} modulation by substrate binding to two binding sites: $k_{on} = k_{ona}/(1 + K_a/[S] + [S]/K_b) + k_{onb}/(1 + K_a/[S] + K_aK_b/[S]^2)$, where K_a and K_b are dissociation constants of the first and second binding sites, k_{ona} and k_{onb} are the values of the IF1 rate constant binding to the enzyme with one or two filled nucleotide binding sites. Control: $k_{ona} = 2\ 10^6 \pm 10^5$ M^{-1} s^{-1}, $K_a = 1.28 \pm 0.25$ μM, $k_{onb} = 1.59\ 10^6 \pm 1.2\ 10^5$ M^{-1} s^{-1}, and $K_b = 75 \pm 60$ μM; PP_i pretreated: $k_{ona} = 2.5\ 10^6 \pm 1.3\ 10^5$ M^{-1} s^{-1}, $K_a = 0.78 \pm 0.11$ μM, $k_{onb} = 1.95\ 10^6 \pm 8\ 10^4$ M^{-1} s^{-1}, and $K_b = 32 \pm 20$ μM.

analyzed as described in ref *39*, showing a monoexponential decay of ATPase activity. The apparent deactivation rate constant (k_{app}) was obtained from the fit.

Chemicals and Reagents. All reagents were of analytical grade. Nucleotides, NADH, pyruvate kinase (sulfate-free), and lactate dehydrogenase (sulfate-free) were obtained from Roche (Basel, Switzerland).

RESULTS

Effect of PP_i Pretreatment on Catalytic Properties of F_1-ATPase. Pyrophosphate pretreatment of nucleotide-depleted F_1-ATPase is known to mimic ATP binding to noncatalytic sites (*40*). Figure 1 shows the steady-state rate of ATP hydrolysis by the control and PP_i-pretreated F_1-ATPase as a function of MgATP concentration. PP_i pretreatment increases ATPase activity at any MgATP concentration. ATPase activity without PP_i pretreatment, previously studied for MgATP concentrations up to 1 mM, had been considered practically Michaelian with $K_m = 55$ μM (*39*). Here, we show that at higher MgATP concentrations (up to 20 mM) the ATPase activity actually continues to rise (Figure 1). After PP_i pretreatment, this phase is minimized, and ATPase activity converges to the same value as that of the control at saturating MgATP concentration. With respect to previous analysis (*39*), saturation curve modeling requires a new component of low affinity. This component increases activity by almost 40% (control) or by about 9% (PP_i-pretreated enzyme). Also, we found that the addition of a third (minor) component in the micromolar range significantly improved the fit, and finally, three components of different affinities were used. These parameters are indicated in the legend to Figure 1. Because of its minor role, the parameters of the first component (K_1, υ_1) cannot be precisely determined. The dissociation constant of the second component (K_2, υ_2) grossly corresponds to K_m in our previous work (*39*). The third component (K_3, υ_3), responsible for the increase of ATPase activity above 1 mM, without concomitant decrease of βW345 fluorescence (see below), cannot be due to the filling of a catalytic site. We verified that it could not be mimicked by increasing ionic strength (not shown). This rise in ATPase activity is likely due to the filling of one or several noncatalytic sites. These data and their interpretation are consistent with some previous reports (*13*, *48*) but deviate from other data obtained with *E. coli* F_1-ATPase, where a single K_d (ADP) value of 25 μM was found for the three noncatalytic sites (*14*). PP_i treatment did not fully abolish the low affinity component of ATPase kinetics (Figure 1). This could be due to some release of PP_i from the low affinity noncatalytic sites after diluting F_1-ATPase in the reaction medium. This has a very limited effect on the determination of kinetic parameters. Importantly, the lag time typically observed in the ATP hydrolysis progression curves at intermediate MgATP concentrations (0.01−1 mM) completely disappeared after PP_i pretreatment (data not shown), as expected (*13*).

Because of the nucleotide content of the ATP-regenerating system, MgATP concentrations in Figure 1 might be underestimated by, at most, 50 nM. Increasing MgATP concentration by 50 nM only affects the parameters of the high affinity component, and the changes are meaningless because the values of K_1 and υ_1 remain within the error interval, which is large.

Effect of Pyrophosphate Pretreatment on the Kinetics of ATPase Inhibition by IF1. We added IF1 (20 nM) to F_1-ATPase during steady-state hydrolysis and observed as we did previously the time-dependent decay of ATPase activity. This decay could be fitted to a monoexponential model (*39*), and the IF1 kinetic binding constant (k_{on}) deduced from this fit was plotted as a function of MgATP concentration (Figure 2). As previously observed (*39*), k_{on} dramatically increases when MgATP concentration is in the micromolar range and moderately decreases at higher MgATP concentrations. The new fact is that PP_i pretreatment slightly increases k_{on} (by 20−30%) at any MgATP concentration. Taking into account the fact that k_{on} decrease beyond 1 mM MgATP is an unspecific effect of ionic strength (*39*), only data below 1 mM MgATP were fitted to a theoretical model in which k_{on} is modulated by MgATP binding on two sites of different affinities. This gave phenomenological dissociation constants K_a and K_b, representing MgATP concentrations for which the half-rise and the half-decrease of k_{on} are reached. Because of the low magnitude of k_{on} decrease at high MgATP concentrations, only K_a may be really determined. Its value is 1.28 ± 0.25 μM for the control and $K_a = 0.78 \pm 0.11$ μM for the PP_i-treated enzyme. If one considers, as envisaged above, that MgATP concentrations should be corrected by 50 nM, K_a would become 1.40 ± 0.33 μM for the control and 0.92 ± 0.15 μM for PP_i-pretreated F_1-ATPase, which is not significantly different. Because k_{on} probably depends not only on the accessibility of the IF1 binding site but also on the turnover rate (*39*), which is higher with PP_i-pretreated material, we have plotted k_{on} as a function of the enzyme rate of turnover, varied by MgATP concentration (Figure 3). For a given turnover rate, k_{on} is higher with PP_i-pretreated

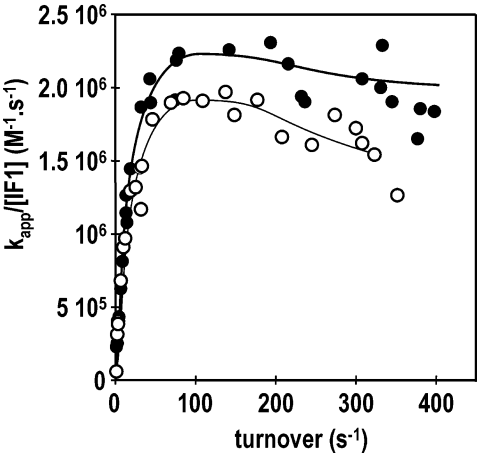

FIGURE 3: Rate constant of inhibition by IF1 as a function of catalytic turnover. Effect of PP_i pretreatment from the data in Figures 1 and 2. (○), control; (●), PP_i pretreated.

material, which shows that k_{on} increase after PP_i pretreatment is not the simple consequence of the stimulation of ATP hydrolysis.

Catalytic Site Occupancy in PP_i-Pretreated F_1-ATPase. Further analysis is required to estimate the catalytic site occupancy during steady-state ATP hydrolysis to know whether it controls the k_{on} value. This may be achieved by measuring the ATP-dependent fluorescence quenching of the mutated residue βW345 (*39*). This technique was first introduced in *E. coli* F_1-ATPase (*46*) and applied to *Bacillus* PS3 F_1-ATPase (*47*, *48*). With mitochondrial F_1-ATPase, which is very active, this approach is possible only for very short reaction times because measurements should be done in the absence of the ATP-regenerating system. In our previous work, because of the lag time of ATPase activity observed at intermediate MgATP concentration, such rapid measurements could be done only at two MgATP concentrations, 1 μM and 1 mM (*39*). In the present work, elimination of the lag time by PP_i pretreatment allows us to do it at any MgATP concentration. Figure 4 shows the fluorescence of PP_i-pretreated βY345W F_1-ATPase as a function of MgATP concentration. Fluorescence was measured within the first 2 s following MgATP addition (see Materials and Methods for details). After 2 s, at the most, 20% of MgATP was hydrolyzed for the lowest substrate concentrations and much less at high concentrations. Several phases of fluorescence decrease are observed, and at high MgATP concentrations, the fluorescence reaches a plateau that represents about 55% of the initial value. This plateau corresponds to the filling of the three catalytic sites. As a comparison, we also studied the filling of catalytic sites of PP_i-pretreated F_1-ATPase by MgADP and MgAMP-PNP (Figure 5). Maximum fluorescence quenching was the same as that with MgATP. Fluorescence data were fitted to a tri-site model with three different dissociation constants K_{d1}, K_{d2}, and K_{d3} (Table 1). Two sets of constants were calculated. It was first assumed that filling of each of the three catalytic sites led to identical fluorescence quenching. The second set of constants was obtained without making this assumption. In both cases, K_{d1} was too small to be measured with MgATP (below nM); K_{d2} was 0.11 ± 0.02 μM in the first case and 0.08 ± 0.03 μM in the second case; and K_{d3} was 50 ± 10 μM in the first case and 41 ± 6 μM in the second case. So the values of

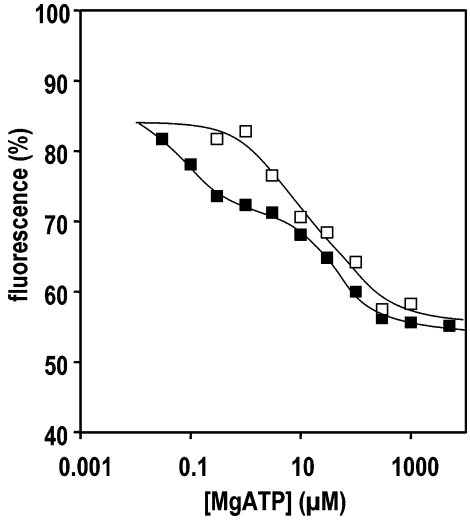

FIGURE 4: Fluorescence of PP_i-pretreated βY345W F_1-ATPase as a function of MgATP concentration. Conditions are as described under Materials and Methods. MF_1 concentrations: 5 nM for 0.03−100 μM MgATP, 10−15 nM for 0.3−1 mM MgATP, and 30 nM for 5 mM MgATP. (■), no IF1 present; (□), 1 μM WT IF1. Fluorescence was integrated on the first 2 s after MgATP addition. Each point represents the average of 10 measurements without IF1 and the average of 5 measurements with IF1. Continuous curves are fits obtained without assuming identical fluorescence quenching for the three sites. Parameters of the fits are displayed in Table 1.

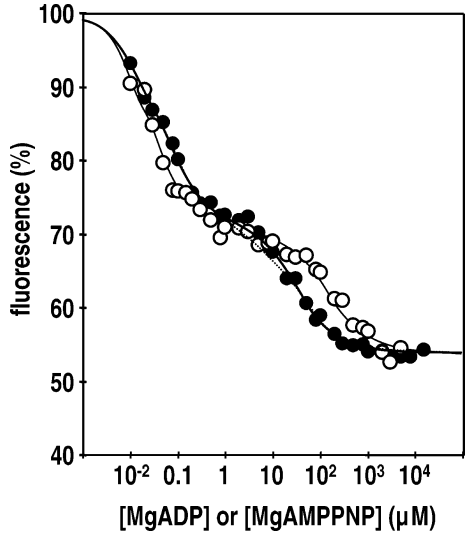

FIGURE 5: Fluorescence of PP_i-pretreated βY345W F_1-ATPase as a function of MgADP (●) and MgAMP-PNP (○) concentrations. Conditions are as described in Materials and Methods. MF_1 concentrations: 10 nM or 30 nM, depending on nucleotide concentration. The values (average of 2−4 measurements) were taken at equilibrium. Continuous curves are fits obtained without assuming identical fluorescence quenching for the three sites. The dotted curve is the fit obtained after imposing identical fluorescence quenching for the three sites (it can be distinguished from the continuous curve only in the case of MgADP). Parameters of the fits are displayed in Table 1.

binding parameters for MgATP depend only a little on the initial postulate. K_d values were obtained using an ordered model for nucleotide binding, but they were practically unchanged if a random mechanism was assumed (not shown).

Table 1 also contains the values of K_{d1}, K_{d2}, and K_{d3} for MgADP and MgAMP-PNP, the values in parentheses being those previously obtained without PP_i pretreatment (*39*). K_{d1}

Table 1: Determination of Nucleotide Binding Parameters from βW345 Fluorescence

substrate	fit	K_{d1} (μM); $\Delta F1$ (%)	K_{d2} (μM); $\Delta F2$ (%)	K_{d3} (μM); $\Delta F3$ (%)
MgATP	single ΔF	<0.001; 14.9 ± 0.2	0.11 ± 0.02; 14.9 ± 0.2	49.9 ± 9.8; 14.9 ± 0.2
	distinct ΔF	<0.001; 15.0 ± 1.8	0.076 ± 0.032; 13.3 ± 1.6	41.3 ± 6.3; 16.8 ± 3.6
MgATP (+IF1)	single ΔF	<0.001; 14.8 ± 0.8	2.7 ± 1.1; 14.8 ± 0.8	97 ± 54; 14.8 ± 0.8
	distinct ΔF	<0.001; 15.9 ± 1.7	3.7 ± 1.7; 15.5 ± 4.5	114 ± 57; 12.7 ± 4.9
MgADP	single ΔF	~0.007; 15.4 ± 0.7 (0.010)	0.18 ± 0.02; 15.4 ± 0.7 (0.22)	44.7 ± 3.9; 15.4 ± 0.7 (16.3)
	distinct ΔF	~0.0002; 7.7 ± 1.4	0.054 ± 0.01; 20.1 ± 1.3	30.3 ± 1.8; 18.5 ± 0.3
MgAMP-PNP	single ΔF	~0.005; 15.3 ± 0.2	0.065 ± 0.007; 20.1 ± 1.3	196 ± 40; 15.3 ± 0.2
	distinct ΔF	<0.001; 9.3 ± 2.9	0.034 ± 0.013; 20.4 ± 3.0	150 ± 39; 16.5 ± 5.8

[a] Catalytic site dissociation constants (K_{d1}, K_{d2}, and K_{d3}) and the magnitude of βW345 fluorescence quenching ($\Delta F1$, $\Delta F2$, and $\Delta F3$) by nucleotide binding to PP_i-pretreated F_1-ATPase are shown. ΔF is expressed as the percentage of the nucleotide-free enzyme fluorescence. Values were calculated from the data in Figure 4 (MgATP, without and with IF1) and Figure 5 (MgADP and MgAMP-PNP) as described under Materials and Methods. Fluorescence intensity is $F = 100[E] + (100 - \Delta F1)[ES_1] + (100 - \Delta F1 - \Delta F2)[ES_1S_2] + (100 - \Delta F1 - \Delta F2 - \Delta F3)[ES_1S_2S_3]$, where E is the nucleotide-free enzyme, and ES_1, ES_1S_2, and $ES_1S_2S_3$ have 1, 2, and 3 filled catalytic sites, respectively. Calculations were made assuming a single value or distinct values for $\Delta F1$, $\Delta F2$, and $\Delta F3$. K_d values in parentheses (MgADP, single ΔF value) were previously obtained with non-PP_i-pretreated F_1-ATPase (*39*).

and K_{d2} values for MgADP were not significantly changed by PP_i-pretreatment, but the K_{d3} value was almost trebled. The latter result slightly differs from that obtained in *E. coli* F_1-ATPase, where PP_i pretreatment did not at all affect MgADP binding to catalytic sites (*49*).

No K_d value for ATP binding matches with the half-rise of k_{on} ($K_a = 0.8 \pm 0.1$ μM) estimated in Figure 2. This corroborates our previous proposal (*39*) that the IF1 binding rate is not directly controlled by the catalytic state of F_1-ATPase. By contrast, K_{d3} (40 ± 6 μM) could match the half-decrease of k_{on} ($K_b = 32 \pm 20$ μM), although the latter is not precisely determined (legend to Figure 2).

Catalytic Sites Occupancy in IF1-Inhibited F_1-ATPase. To investigate the occupancy of the catalytic sites in the IF1-inhibited state of F_1-ATPase, the PP_i-pretreated enzyme was first incubated with 1 μM IF1 for 30 s, a time too short to form ATPase−IF1 complex in the absence of nucleotides (*39*), and then MgATP was added, which triggered ATP hydrolysis and IF1 binding at the same time. βW345 fluorescence quenching was estimated as in control conditions and plotted on the same graph (Figure 4). At any MgATP concentration, the fluorescence quenching, related to the catalytic site nucleotide content, was decreased in the presence of IF1. K_{d2} was increased 25−50-fold, and K_{d3} was increased 2−3-fold (Table 1). This suggests that IF1 binding during ATP hydrolysis diminishes ATP binding.

IF1 Binding to ADP-Loaded F_1-ATPase. It is well established that MgATP is required to promote IF1 binding and that it cannot be replaced by MgAMP-PNP. However, this does not prove that IF1 binds to an ATP-containing catalytic site because during ATP hydrolysis F_1-ATPase also contains ADP. We have estimated the rate of IF1 binding to F_1-ATPase saturated with MgADP by using a method previously developed to detect loose binding of IF1 on the nucleotide-free enzyme (*39*). It consists of incubating resting F_1-ATPase for different times with IF1 at a high concentration and then diluting it in a reaction medium containing MgATP at a high concentration to rapidly trap already bound IF1. Here, PP_i-pretreated F_1-ATPase (50 nM) was incubated for various times with IF1 (100 nM) in the presence of 250 μM MgADP. The binding of IF1 was indirectly probed by measuring ATPase activity just after diluting an aliquot of incubated material in the spectrophotometric cuvette containing the reaction medium. From the dependence of ATPase activity on the incubation time with IF1, k_{on} was estimated to be 2×10^4 M^{-1} min^{-1} (data not shown), about 100 times lower than that in the presence of 250 μM MgATP (see Figure 2). This shows that MgADP-saturated F_1-ATPase binds IF1 very slowly with respect to the MgATP-saturated enzyme.

DISCUSSION

Dynamic Aspects of IF1 Binding. From crystallographic data, IF1 was found to be bound at an α/β catalytic interface, equivalent to the β_{DP} site of the reference state (*5*) with respect to the γ position but apparently filled with ATP instead of ADP (*35*). From a dynamic point of view, it has been known for a long time that ATPase turnover is necessary for IF1 binding (*30*, *37*). The relationship between MgATP concentration and the rate of IF1 binding is complex (*38*−*39*). We previously found a mismatch between the occupancy of the catalytic sites and the rate of IF1 binding (*39*). This analysis was limited by the fact that ATP binding had to be measured within a few seconds, whereas in most cases, steady-state ATP hydrolysis occurred only after several minutes. Therefore, ATP binding parameters were deduced not directly from βW345 fluorescence but from a combination of kinetic and fluorescence assays. Here, freezing the noncatalytic sites by PP_i pretreatment abolished the lag of ATPase activity and allowed for the fast measurement of nucleotide occupancy at all ATP concentrations. The mismatch between ATP binding and IF1 binding was confirmed. This strengthens the view according to which the binding process occurs in two separate steps: (1) IF1 loose binding that depends on the geometry of α/β interfaces, determined by catalytic occupancy and (2) turnover-dependent IF1 locking. In this model, the theoretical value of the rate constant k_{on} is determined by the catalytic state of the enzyme, but the observed value is a macroscopic constant modulated by the competition between IF1 locking and release (*39*).

Role of Noncatalytic Sites. PP_i pretreatment, which mimics the filling of noncatalytic sites by ATP (*13*, *40*), slightly increases the rate of IF1 binding, independent of the enhancement of the catalytic turnover. One may speculate that filling noncatalytic sites with ATP directly acts on the

accessibility of IF1 binding sites. Our kinetic data strongly suggest that at least two classes of noncatalytic sites bind ATP with different affinities, one below 100 μM (this work and refs *13* and *40*) and another above 1 mM. Because PP_i pretreatment accelerates IF1 binding at MgATP concentrations that saturate the noncatalytic sites of higher affinity, it is logical to suppose that this effect is due to conformational change of the noncatalytic sites of lower affinity. But it cannot be excluded that PP_i pretreatment affects the rate of IF1 binding by a specific mechanism. Unfortunately, it is not possible to study the effect of PP_i pretreatment on IF1 binding at MgATP concentrations above millimolar because at these concentrations, the effect of ionic strength on k_{on} becomes predominant. Whatever the precise mechanism is, the conformation of noncatalytic sites modulates the accessibility of IF1 binding site only a little. We are not sure that such a limited effect could be detected by structural investigations.

Going Deeper into the Bind−Lock Mechanism of IF1. IF1 binds very slowly to nucleotide-free (*39*) and to ADP-loaded (this work) F_1-ATPase. Although we do not know the structure of these two forms of F_1-ATPase, it is plausible that at least one of the catalytic sites of the nucleotide-free species and one of the sites of the ADP-loaded species look like the empty and the ADP-filled catalytic sites, respectively, of the working enzyme. It is therefore probable that during ATP hydrolysis IF1 only binds to a catalytic site occupied by ATP. IF1 could loosely bind to this site when it is not yet tightly closed and would be locked during tight closing promoted by catalytic events on other sites.

Nucleotide analysis of IF1-inhibited F_1-ATPase (*50*) and crystallographic study of bovine F_1-ATPase in complex with IF1 (*35*) suggest that IF1 inhibits the cleavage of ATP into ADP and Pi. We showed here that catalytic site occupancy decreases in the IF_1-inhibited F_1-ATPase. It was previously shown that depending on MgATP concentration present before inhibition IF1-inhibited F_1-ATPase, but not the active enzyme, retained up to one catalytic nucleotide after separation from unbound nucleotides (*50*). Our present data do not contradict this report because here we measured bound nucleotides in equilibrium with free nucleotides in the medium. Within the investigated MgATP concentration range, the minimum amount of catalytic nucleotides after IF1 inhibition here is about 1 per F_1-ATPase (Figure 4), which could correspond to the previously detected entrapped nucleotide (*50*). The decrease in affinity for nucleotides in the IF1-inhibited complex only concerns the second and the third catalytic sites, mainly the second one (Table 1). These data may be simply rationalized (Figure 6). During multisite ATP hydrolysis, ATP loose binding to site (−1) promotes ATP hydrolysis at site (0), which in turn would fully close site (−1), and also opens site (+1), which eventually contains ADP. By inhibiting ATP hydrolysis at site (0), bound IF1 prevents this interconversion between closed and open sites. At low ATP concentration, site (+1) is empty because ADP release from this site, although slow, preceded ATP binding to site (−1). The only effect of IF1 on nucleotide occupancy is to decrease bound ATP, which results in a 25−50-fold increase in K_{d2} (Table 1). At high ATP concentration, site (+1) is occupied by ADP, and in addition to decreasing bound ATP, IF1 increases bound ADP. This results in a modest increase in K_{d3} (2−3-fold).

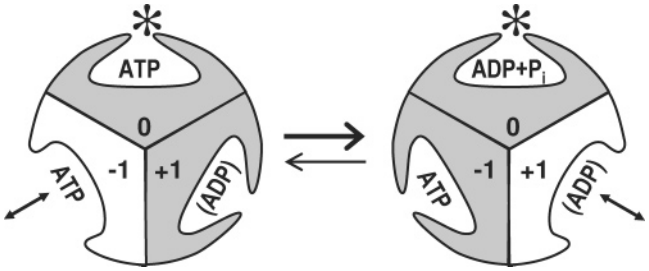

FIGURE 6: IF1 inhibition and nucleotide occupancy. The two catalytic states are before (left) and after (right) ATP hydrolysis on site (0). ATP hydrolysis converts site (−1) from a loose site to a tight site and site (+1) from a tight site to a loose site. IF1 bound to site (0) during a previous catalytic cycle (asterisk) prevents ATP hydrolysis and also conformation changes of sites (−1) and (+1). Parentheses indicate that site (+1) contains ADP only at high ATP concentrations. See text for details.

According to our data and this mechanism, the average number of nucleotides of the dead-end IF1−ATPase complex is variable, whereas the crystallized IF1−ATPase complex has two bound nucleotides (*35*). It is probable that inhibited enzymes with different nucleotide occupancy slowly converge to a unique state before or during crystallization.

The proposal that IF1 loosely binds to an ATP-containing interface may simply explain why IF1 is not retained to the enzyme during pmf-driven ATP synthesis. If IF1 indeed binds to this interface during ATP synthesis, the next state experienced by this site is the open, nucleotide-free state, which probably has a very high k_{off} for IF1 and therefore allows its release. This model provides a clue for understanding the unidirectional character of mitochondrial ATP synthase inhibition by IF1.

Bi-Site versus Tri-Site Catalysis. Our data are consistent with tri-site ATP hydrolysis, a model supported in all the reports using tryptophan to probe the filling of catalytic sites, using F_1-ATPase from *E. coli* (*46*, *51*) as well as from *Bacillus* PS3 (*47*, *48*). In contrast, data obtained on bovine F_1-ATPase by a rapid filtration technique supported bi-site ATP hydrolysis (*52*), but they were questioned in a later report (*53*). Fluorescence data from Figures 4 and 5 could actually be fitted using a bi-site model by assuming that the two sites do not equally contribute to βY345 fluorescence (not shown). The resulting dissociation constants for MgATP would be $K_{d1} = 15$ nM and $K_{d2} = 34$ μM. Again, none of these constants match with the half-rise of the IF1 binding rate ($K_a = 0.8$ μM), and the bind−lock mechanism remains valid.

The bi-site model would imply that the βW345 fluorescence plateau around 1 μM MgATP corresponds to the filling of a single catalytic site (Figure 4). However, the catalytic turnover in this MgATP concentration range is about 15−20 s^{-1} (Figure 1). Even with the small contribution of sites of intermediate affinity, this is inconsistent with the much lower single site catalytic turnover (0.05 s^{-1} to 0.1 s^{-1}) reported for the bovine (*54*−*55*) and yeast (*56*) mitochondrial F_1-ATPases. It is therefore highly probable that the transient plateau of βW345 fluorescence observed in the micromolar ATP concentration range is due to the saturation of the second catalytic site. In conclusion, even though we consider that some caution is still mandatory, we regard the tri-site mechanism as the most probable one.

ACKNOWLEDGMENT

Excellent technical help was provided by Véronique Mary. We are indebted to Gwénaëlle Moal-Raisin for expertise in molecular biology. We thank Dr. David M. Mueller (Chicago, IL) for providing us with the plasmid pRS344SB.

REFERENCES

1. Boyer, P. D. (1997) The ATP synthase: a splendid molecular machine, *Annu. Rev. Biochem. 66*, 717−749.
2. Moser, T. L., Kenan, D. J., Ashley, T. A., Roy, J. A., Goodman, M. D., Misra, U. K., Cheek, D. J., and Pizzo, S. V. (2001) Endothelial cell surface F_1-F_0 ATP synthase is active in ATP synthesis and is inhibited by angiostatin, *Proc. Natl. Acad. Sci. U.S.A. 98*, 6656−6661.
3. Mitchell, P. (1961) Coupling of phosphorylation to electron and hydrogen transfer by a chemi-osmotic type of mechanism, *Nature 191*, 144−148.
4. Mitchell, P. (1977) A commentary on alternative hypotheses of protonic coupling in the membrane systems catalysing oxidative and photosynthetic phosphorylation, *FEBS Lett. 78*, 1−20.
5. Abrahams, J. P., Leslie, A. G., Lutter, R., and Walker, J. E. (1994) Structure at 2.8 Å resolution of F_1-ATPase from bovine heart mitochondria, *Nature 370*, 621−628.
6. Velours, J., Paumard, P., Soubannier, V., Spannagel, C., Vaillier, J., Arselin, G., and Graves, P.-V. (2000) Organisation of the yeast ATP synthase F_0: a study based on cysteine mutants, thiol modification and cross-linking reagents, *Biochim. Biophys. Acta 1458*, 443−456.
7. Rubinstein, J. L, Walker J, E., and Henderson, R. (2003) Structure of the mitochondrial ATP synthase by electron cryomicroscopy, *EMBO J. 22*, 6182−6192.
8. Duncan, T. M., Bulygin, V. V., Zhou, Y., Hutcheon, M. L., and Cross, R. L. (1995) Rotation of subunits during catalysis by *Escherichia coli* F_1-ATPase, *Proc. Natl. Acad. Sci. U.S.A. 92*, 10964−10968.
9. Noji, H., Yasuda, R., Yoshida, M., and Kinosita, K. Jr. (1997) Direct observation of the rotation of F_1-ATPase, *Nature 386*, 299−302.
10. Cross, R. L., and Nalin, C. M. (1982) Adenine nucleotide binding sites on beef heart F_1-ATPase. Evidence for three exchangeable sites that are distinct from three noncatalytic sites, *J. Biol. Chem. 257*, 2874−2881.
11. Di Pietro, A., Godinot, C., and Gautheron, D. C. (1981) Interaction between catalytic and regulatory sites of mitochondrial F_1 adenosine-5′-triphosphatase as monitored by the differential effects of inhibitors and nucleotide analogues on the 'hysteretic' behavior of the enzyme, *Biochemistry 20*, 6312−6318.
12. Harris, D. A. (1993) The 'non-exchangeable' nucleotides of F_1-F_0ATP synthase. Cofactors in hydrolysis? *FEBS Lett. 316*, 209−215.
13. Jault, J.-M., and Allison, W. S. (1994) Hysteretic inhibition of the bovine heart mitochondrial F_1-ATPase is due to saturation of noncatalytic sites with ADP which blocks activation of the enzyme by ATP, *J. Biol. Chem. 269*, 319−325.
14. Weber, J., Wilke-Mounts, S., Grell, E., and Senior, A. E. (1994) Tryptophan fluorescence provides a direct probe of nucleotide binding in the noncatalytic sites of *Escherichia coli* F_1-ATPase, *J. Biol. Chem. 269*, 11261−11268.
15. Ren, H., and Allison, W. S. (2000) Substitution of βGlu^{201} in the $\alpha_3\beta_3\gamma$subcomplex of the F_1-ATPase from the thermophilic *Bacillus* PS3 increases the affinity of catalytic sites for nucleotides, *J. Biol. Chem. 275*, 10057−10063.
16. Falson, P., Goffeau, A., Boutry, M., Jault, J.-M. (2004) Structural insight into the cooperativity between catalytic and noncatalytic sites of F_1-ATPase, *Biochim. Biophys. Acta 1658*, 133−140.
17. Yasuda, R., Noji, H., Yoshida, M., Kinosita, K. Jr., and Itoh, H. (2001) Resolution of distinct rotational substeps by submillisecond kinetic analysis of F_1-ATPase, *Nature 410*, 898−904.
18. Nishizaka, T., Oiwa, K, Noji, H., Kimura, S., Muneyuki, E., Yoshida, M., and Kinosita, K., Jr. (2004) Chemomechanical coupling in F_1-ATPase revealed by simultaneous observation of nucleotide kinetics and rotation, *Nat. Struct. Mol. Biol. 11*, 142−148.
19. Pullman, M. E., and Monroy, G. C. (1963) A naturally occurring inhibitor of mitochondrial adenosine triphosphatase, *J. Biol. Chem. 238*, 3762−3768.
20. Matsubara, H., Hase, T., Hashimoto, T., and Tagawa, K. (1981) Amino acid sequence of an intrinsic inhibitor of mitochondrial ATPase from yeast, *J. Biochem. (Tokyo) 90*, 1159−1165.
21. Norling, B., Tourikas, C., Hamasur, B., and Glaser, E. (1990) Evidence for an endogenous ATPase inhibitor protein in plant mitochondria. Purification and characterization, *Eur. J. Biochem. 188*, 247−252.
22. Cabezón, E., Runswick, M. J., Leslie, A. G., and Walker J. E. (2001) The structure of bovine IF1, the regulatory subunit of mitochondrial F-ATPase, *EMBO J. 20*, 6990−6996.
23. Schwerzmann, K., and Pedersen, P. L. (1986) Regulation of the mitochondrial ATP synthase/ATPase complex, *Arch. Biochem. Biophys. 250*, 1−18.
24. Van de Stadt, R. J., de Boer, B. L., and Van Dam, K. (1973) The interaction between the mitochondrial ATPase (F_1) and the ATPase inhibitor, *Biochim. Biophys. Acta 292*, 338−349.
25. Husain, I., and Harris, D. A. (1983) ATP synthesis and hydrolysis in submitochondrial particles subjected to an acid-base transition. Effects of the ATPase inhibitor protein, *FEBS Lett. 160*, 110−114.
26. Power, J., Cross, R. L., and Harris, D. A. (1983) Interaction of F_1-ATPase from ox heart mitochondria with its naturally occurring inhibitor protein. Studies using radio-iodinated inhibitor protein, *Biochim. Biophys. Acta 724*, 128−141.
27. Klein, G., and Vignais, P. V. (1983) Effect of the protonmotive force on ATP-linked processes and mobilization of the bound natural ATPase inhibitor in beef heart submitochondrial particles, *J. Bioenerg. Biomembr. 15*, 347−362.
28. Husain, I., Jackson, P. J., and Harris, D. A. (1985) Interaction between F_1-ATPase and its naturally occurring inhibitor protein. Studies using a specific anti-inhibitor antibody, *Biochim. Biophys. Acta 806*, 64−74.
29. Lippe, G., Sorgato, M. C., and Harris, D. A. (1988) Kinetics of the release of the mitochondrial inhibitor protein. Correlation with synthesis and hydrolysis of ATP, *Biochim. Biophys. Acta 933*, 1−11.
30. Lippe, G., Sorgato, M. C., and Harris, D. A. (1988) The binding and release of the inhibitor protein are governed independently by ATP and membrane potential in ox-heart submitochondrial vesicles, *Biochim. Biophys. Acta 933*, 12−21.
31. Venard, R., Brèthes, D., Giraud, M.-F., Vaillier, J., Velours, J., and Haraux, F. (2003) Investigation of the role and mechanism of IF1 and STF1 proteins, twin inhibitory peptides which interact with the yeast mitochondrial ATP synthase, *Biochemistry 42*, 7626−7636.
32. Dreyfus, G., Gómez-Puyou, A., and de Gómez-Puyou, M. T. (1981) Electrochemical gradient induced displacement of the natural ATPase inhibitor protein from mitochondrial ATPase as directed by antibodies against the inhibitor protein, *Biochem. Biophys. Res. Commun. 100*, 400−406.
33. Beltran, C., de Gómez-Puyou, M. T., Gómez-Puyou, A., and Darszon, A. (1984) Release of the inhibitory action of the natural ATPase inhibitor protein on the mitochondrial ATPase, *Eur. J. Biochem. 144*, 151−157.
34. Lopez-Mediavilla, C., Vigny, H., and Godinot, C. (1993) Docking the mitochondrial inhibitor protein IF1 to a membrane receptor different from the F_1-ATPase beta subunit, *Eur. J. Biochem. 215*, 487−496.
35. Cabezón, E., Montgomery, M. G., Leslie, A. G., and Walker, J. E. (2003) The structure of bovine F_1-ATPase in complex with its regulatory protein IF1, *Nat. Struct. Biol. 10*, 744−750.
36. Gibbons, C., Montgomery, M. G., Leslie, A. G., and Walker, J. E. (2000) The structure of the central stalk in bovine F_1-ATPase at 2.4 Å resolution, *Nat. Struct. Biol. 7*, 1055−1061.
37. Klein, G., Satre, M., and Vignais, P. (1977) Natural protein ATPase inhibitor from *Candida utilis* mitochondria. Binding properties of the radiolabeled inhibitor, *FEBS Lett. 84*, 129−134.
38. Milgrom, Y. M. (1989) An ATP dependence of mitochondrial F_1-ATPase inactivation by the natural inhibitor protein agrees with the alternating-site binding-change mechanism, *FEBS Lett. 246*, 202−206.
39. Corvest, V., Sigalat, C., Venard, R., Falson, P., Mueller, D. M., and Haraux, F. (2005) The binding mechanism of the yeast F_1-ATPase inhibitory peptide: role of catalytic intermediates and enzyme turnover, *J. Biol. Chem. 280*, 9927−9936.
40. Milgrom, Y. M., and Cross, R. L. (1993) Nucleotide binding sites on beef heart mitochondrial F_1-ATPase. Cooperative interactions

between sites and specificity of noncatalytic sites, *J. Biol. Chem. 268*, 23179−23185.
41. Sambrook, J., Fritsch, E. F., and Maniatis, T. (1989) In *Molecular Cloning: A Laboratory Manual* (Nolan, C., Ed.) 2nd ed., Cold Spring Harbor Laboratory, Cold Spring Harbor, NY.
42. Shen, H., Yao, B. Y., and Mueller, D. M. (1994) Primary structural constraints of P-loop of mitochondrial F_1-ATPase from yeast, *J. Biol. Chem. 269*, 9424−9428.
43. Gietz, R. D., Schiestl, R. H., Willems, A. R., and Woods, R. A. (1995) Studies on the transformation of intact yeast cells by the LiAc/SS-DNA/PEG procedure, *Yeast 11*, 355−360.
44. Falson, P., Di Pietro, A., and Gautheron, D. C. (1986) Chemical modification of thiol groups of mitochondrial F_1-ATPase from the yeast *Schizosaccharomyces pombe*. Involvement of α- and γ-subunits in the enzyme activity, *J. Biol. Chem. 261*, 7151−7159.
45. Senior, A. E., Lee, R. S., al-Shawi, M. K., and Weber, J. (1992) Catalytic properties of *Escherichia coli* F_1-ATPase depleted of endogenous nucleotides, *Arch. Biochem. Biophys. 297*, 340−344.
46. Weber, J., Wilke-Mounts, S., Lee, R. S., Grell, E., and Senior, A. E. (1993) Specific placement of tryptophan in the catalytic sites of *Escherichia coli* F_1-ATPase provides a direct probe of nucleotide binding: maximal ATP hydrolysis occurs with three sites occupied, *J. Biol. Chem. 268*, 20126−20133.
47. Dou, C., Fortes, P. A., and Allison, W. S. (1998) The $\alpha_3(\beta Y341W)_3\gamma$ subcomplex of the F_1-ATPase from the thermophilic *Bacillus* PS3 fails to dissociate ADP when MgATP is hydrolyzed at a single catalytic site and attains maximal velocity when three catalytic sites are saturated with MgATP, *Biochemistry 37*, 16757−16764.
48. Ono, S., Hara, K. Y., Hirao, J., Matsui, T., Noji, H., Yoshida, M., and Muneyuki, E. (2003) Origin of apparent negative cooperativity of F_1-ATPase, *Biochim. Biophys. Acta 1607*, 35−44.
49. Weber, J., and Senior, A. E. (1995) Location and properties of pyrophosphate-binding sites in *Escherichia coli* F_1-ATPase, *J. Biol. Chem. 270*, 12653−12658.
50. Milgrom, Y. M. (1991) When beef-heart mitochondrial F_1-ATPase is inhibited by inhibitor protein a nucleotide is trapped in one of the catalytic sites, *Eur. J. Biochem. 200*, 789−795.
51. Weber, J., and Senior, A. E. (2001) Bi-site catalysis in F_1-ATPase: does it exist?, *J. Biol. Chem. 276*, 35422−35428.
52. Milgrom, Y. M., and Cross, R. L. (2005) Rapid hydrolysis of ATP by mitochondrial F_1-ATPase correlates with the filling of the second of three catalytic sites, *Proc. Natl. Acad. Sci. U.S.A. 102*, 13831−13836.
53. Ren, H., Bandyopadhyay, S., and Allison, W. S. (2006) The $\alpha_3(\beta Met^{222}Ser/Tyr^{345}Trp)_3\gamma$ subcomplex of the TF_1-ATPase does not hydolyze ATP at a significant rate until the substrate binds to the catalytic site of the lowest affinity, *Biochemistry 45*, 6222−6230.
54. Milgrom, Y. M., and Murataliev, M. B. (1987) Steady-state rate of F_1-ATPase turnover during ATP hydrolysis by the single catalytic site, *FEBS Lett. 212*, 63−67.
55. Milgrom, Y. M., and Cross, R. L. (1997) Nucleotide-depleted beef heart F_1-ATPase exhibits strong positive catalytic cooperativity, *J. Biol. Chem. 272*, 32211−32214.
56. Konishi, J., Yohda, M., Hashimoto, T., and Yoshida, M. (1987) Single site catalysis of the F_1-ATPase from *Saccharomyces cerevisiae* and the effect of inorganic phosphate on it, *J. Biochem. (Tokyo) 102*, 273−279.

BI700522V